Journal of Biomedical Optics

SPIEDigitalLibrary.org/jbo

In vivo photoacoustic microscopy with 7.6-μm axial resolution using a commercial 125-MHz ultrasonic transducer

Chi Zhang
Konstantin Maslov
Junjie Yao
Lihong V. Wang

In vivo photoacoustic microscopy with 7.6-μm axial resolution using a commercial 125-MHz ultrasonic transducer

Chi Zhang, Konstantin Maslov, Junjie Yao, and Lihong V. Wang
Washington University in St. Louis, Department of Biomedical Engineering, Optical Imaging Laboratory, One Brookings Drive, St. Louis, Missouri 63130

Abstract. Photoacoustic microscopy has achieved submicron lateral resolution, but its axial resolution is much lower. Here an axial resolution of 7.6 μm, the highest axial resolution validated by experimental data, has been achieved by using a commercial 125 MHz ultrasonic transducer for signal detection followed by the Wiener deconvolution for signal processing. Limited by the working distance, the high-frequency ultrasonic transducer can penetrate 1.2 mm into biological tissue from the ultrasound detection side. At this depth, the signal-to-noise ratio decreases by 11 dB, and the axial resolution degrades by 36%. The new system was demonstrated in imaging melanoma cells *ex vivo* and mouse ears *in vivo*. [DOI: 10.1117/1.JBO.17.11.116016]

Keywords: photoacoustic microscopy; axial resolution; high-frequency ultrasonic transducer; deconvolution.

Paper 12446 received Jul. 13, 2012; revised manuscript received Oct. 5, 2012; accepted for publication Oct. 15, 2012; published online Nov. 2, 2012.

1 Introduction

Photoacoustic microscopy (PAM) images optical absorption ultrasonically with 100% sensitivity.[1] By exciting biomolecules at appropriate optical wavelengths, PAM can provide rich endogenous contrasts *in vivo*, including hemoglobin, melanin, DNA, RNA, cytochrome, myoglobin, bilirubin, water, and lipid.[2–9] In fact, any molecules, which are absorbing at certain wavelengths, can potentially be imaged by PAM. Moreover, PAM has the unique advantage in imaging the functional parameters associated with these biomolecules, such as imaging hemoglobin oxygen saturation, blood flow speed, and temperature variation.[10–12] Therefore, label-free PAM is expected to join the mainstream optical microscopy technologies.

Spatial resolution is a key parameter of microscopy. For optical-resolution (OR-) PAM, the lateral resolution, provided by the optical focusing, can be estimated as 0.51 λ/NA,[1] where λ is the optical wavelength and NA is the numerical aperture of the optical objective. Submicron lateral resolution has been achieved for OR-PAM.[13,14] The axial resolution, provided by the time-resolved ultrasonic detection, can be estimated, if the impulse response of the ultrasonic transducer has a Gaussian envelope, as 0.88 c/B (see Appendix), where c is the speed of sound and B is the ultrasonic transducer bandwidth, which is approximately proportional to the central frequency. Increasing the bandwidth for better axial resolution will decrease the maximum imaging depth, because higher frequency ultrasound attenuates faster in biological tissues. So far, ~15-μm axial resolution for depths up to 1.2 mm has been reported, using the piezoelectric ultrasonic transducer with a 75 MHz central frequency and a 100 MHz bandwidth.[15,16] Nevertheless, the axial resolution remains much lower than the lateral resolution in OR-PAM.

Besides piezoelectric ultrasonic transducers, optical sensors have been used for the ultrasonic detection, such as microring resonators[17] and Fabry-Perot sensors.[18] With broad bandwidth and low noise, microring resonators help achieve an axial resolution of 8 μm,[17] which, to the best of our knowledge, is the highest axial resolution achieved so far. However, a microring resonator is unfocused, so, in spite of its high sensitivity to acoustic pressure, it generates images with lower quality than a focused piezoelectric transducer in a confocal arrangement.[19] Further, the 8 μm axial resolution has not been demonstrated in biological samples. Moreover, the microring resonator has not been commercialized yet, so it is not readily available to researchers.

The work reported in this paper aims to improve the axial resolution of PAM. By using a commercial 125 MHz ultrasonic transducer for signal detection and the Wiener deconvolution method for signal processing, the axial resolution has reached 7.6 μm, which was experimentally validated. As example applications, we implemented high-axial-resolution imaging of melanoma cells *ex vivo* and mouse ears *in vivo*.

2 Methods

2.1 *Experimental System*

The experimental PAM system is shown in Fig. 1. A tunable OPO laser (NT242-SH, Ekspla) generated laser pulses (5-ns pulse width, 1 kHz pulse repetition rate) with 532-nm wavelength. The laser pulses were spatially filtered by a 50 μm pinhole and then focused by a 0.32-NA objective, providing ~0.8 μm lateral resolution. The laser pulse intensity was measured by a photodiode (SM05PD1A, Thorlabs) to compensate

Address all correspondence to: Lihong V. Wang, Washington University in St. Louis, Department of Biomedical Engineering, Optical Imaging Laboratory, One Brookings Drive, St. Louis, Missouri 63130. Tel: (314) 935-6152; Fax: (314) 935-7448; E-mail: lhwang@wustl.edu

0091-3286/2012/$25.00 © 2012 SPIE

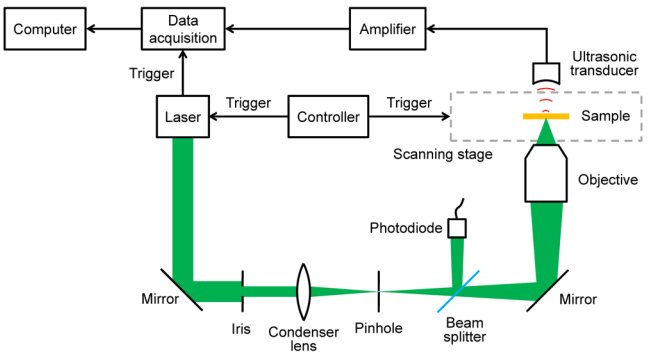

Fig. 1 Schematic of the PAM system.

for the intensity fluctuation. The photoacoustic waves excited by the focused laser pulse were detected by an ultrasonic transducer (125 MHz central frequency, 100 MHz bandwidth, 15 Pa noise equivalent pressure in the 100 MHz bandwidth; V2062, Olympus NDT) with a focusing acoustic lens (NA 0.8). The photoacoustic signals were amplified and digitized at 1 GS $\cdot$ s^{-1} (PCI-5152, National Instruments). The sample was mounted on a scanning stage (PLS-85, MICOS). Both the laser and the scanning stage were triggered by a homemade controller, and the data acquisition card was triggered by the laser output for synchronization. Each time-resolved photoacoustic signal was converted to a 1-D depth-resolved image, and the sample was mechanically scanned in 2-D to generate a three-dimensional (3-D) image.

2.2 *Signal Processing*

To convert each photoacoustic signal to a depth-resolved image, the Hilbert transformation is normally used to extract the envelope of the short-pulsed photoacoustic signal. However, as shown in the literature, deconvolution methods can further improve the axial (depth) resolution.[14] Defining the photoacoustic signal from a point target to be the system impulse response, any photoacoustic signal can be approximately modeled as the convolution of the system impulse response and the depth-resolved target function. Deconvolving the photoacoustic signal with the system impulse response exactly recovers the target function under perfect conditions, a linear and shift-invariant system with no noise. In other words, deconvolution recovers the attenuated frequency components of the signal and broadens the system bandwidth, thereby improving the axial resolution. In practice, however, deconvolution is very sensitive to noise, because the frequency components of the signal outside the system passband may be too weak to be recovered in the presence of noise. Therefore, the improvement of axial resolution by using deconvolution is limited, depending on the signal-to-noise ratio (SNR). In this paper, the Wiener deconvolution method[20] was used for imaging, and the results were compared with those using the Hilbert transformation method.

3 Results

3.1 *System Characterization*

We estimated the axial resolution of the PAM system. The experimental sample was a thin layer of red ink from a whiteboard marker applied to a microscope slide. The photoacoustic waves were excited at the optical focal point on the ink, which worked as a point target for the ultrasonic transducer. The received photoacoustic signal is defined as the system impulse response, as shown in Fig. 2(a). On one hand, the axial resolution can be estimated by the pulse width of the impulse response. The envelope of the impulse response was extracted from the data in Fig. 2(a). The full-width at half-maximum (FWHM) of the envelope is 9 ns, corresponding to 13.5 μm in distance. So the axial resolution is 13.5 μm, which is the size of the image of a point target in the depth direction. This value agrees with that predicted by the axial resolution formula for a Gaussian-enveloped impulse response (see Appendix): 0.88 c/B = 13.2 μm. On the other hand, taking into account that the photoacoustic signals from two point targets add in amplitude instead of in envelope, two targets at a separation smaller than 13.5 μm may still be distinguishable in the image. Then the axial resolution can be estimated by numerically shifting and summing two impulse responses in amplitude and checking whether the two peaks can be differentiated in envelope.[14] Defining the difference in the photoacoustic envelope between the smaller of the two peaks and the valley to be the contrast,[21] the contrast-to-noise ratio (CNR) was plotted versus the shift between the two impulse responses, as shown in Fig. 2(b). The axial resolution, defined as the shift when CNR reaches 6 dB, is 9.5 μm.

We also designed a novel experiment to measure the axial resolution of the PAM system. As shown in Fig. 3(a), the sample to be imaged consisted of two layers of red ink, one on the polymethylpentene (TPX) plastic and the other on the glass slide. A small angle between the TPX plastic and the glass slide provided continuously variable distance between the two layers. The acoustic impedance of the TPX plastic is close to that of water, so the TPX plastic did not block the ultrasound to be

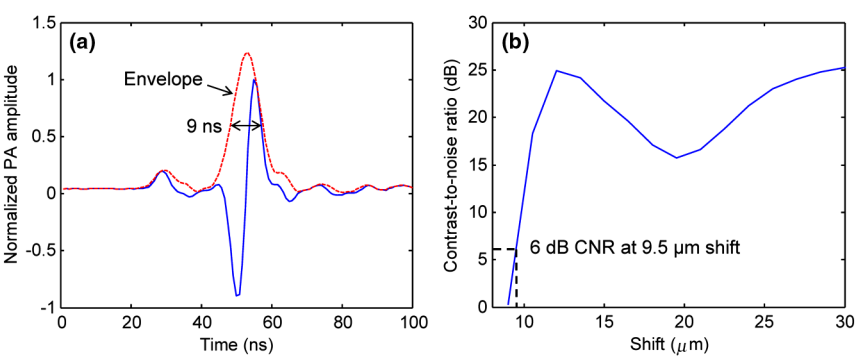

Fig. 2 Estimating the axial resolution of PAM. (a) System impulse response. The full-width at half-maximum (FWHM) of the envelope is 9 ns, corresponding to 13.5 μm in distance. (b) The contrast-to-noise ratio (CNR) versus the shift when summing two impulse responses, as shown in (a).

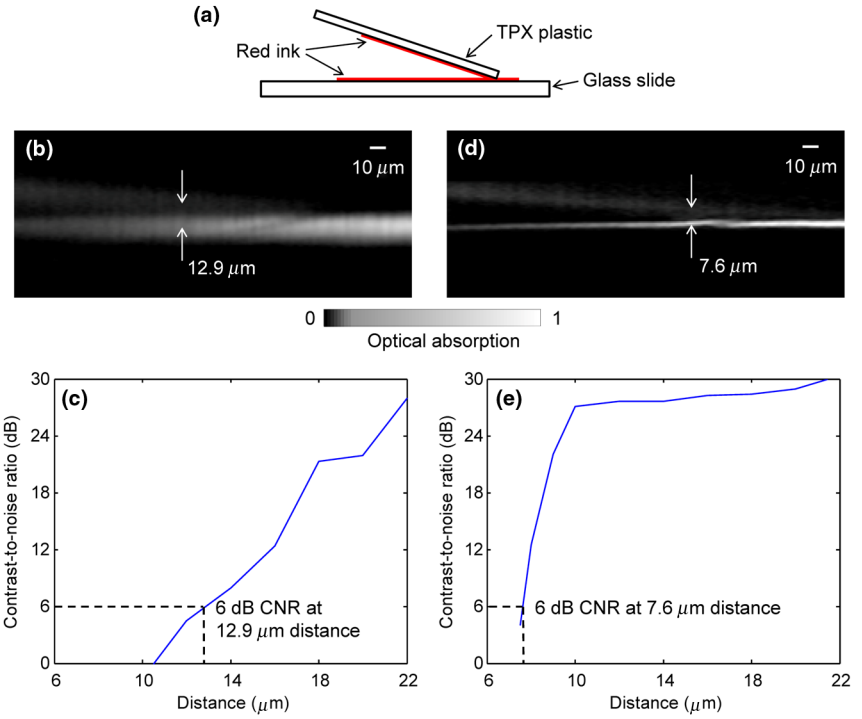

Fig. 3 Experimentally measuring the axial resolution of PAM. (a) The sample to be imaged consists of two layers of red ink on polymethylpentene (TPX) plastic (upper) and glass slide (lower), respectively. (b) The *B*-scan image of the sample calculated by the Hilbert transformation method. (c) The CNR versus the distance between the two layers of (b). The axial resolution is 12.9 μm by using the Hilbert transformation. (d) The *B*-scan image of the sample calculated by the deconvolution method. (e) The CNR versus the distance between the two layers of (d). The axial resolution is 7.6 μm by using the deconvolution.

received by the ultrasonic transducer placed on the top. The TPX plastic and the glass slide were coupled with ultrasound gel. A *B*-scan image of the sample calculated by the Hilbert transformation method is shown in Fig. 3(b). Note that the bottom layer of ink appears brighter in the image, because the light illuminates from the bottom. The CNR versus the distance between the two layers is shown in Fig. 3(c). The axial resolution, given by the distance with 6-dB CNR, is 12.9 μm. This is worse than the theoretical estimation given by the shift-and-sum definition (9.5 μm), likely because the top layer has a much weaker amplitude than the bottom layer and is therefore easier to be mixed into the bottom layer in the image.

As explained above, the Wiener deconvolution method can be used to improve the axial resolution. The *B*-scan image calculated by the deconvolution method is shown in Fig. 3(d). Both layers appear sharper than those in Fig. 3(b). The axial resolution is 7.6 μm, shown in Fig. 3(e), ~1.7 times better than the result from the Hilbert transformation method. With a higher SNR, we expect to achieve an even better axial resolution. Thus, the deconvolution method was used in the following imaging experiments.

We measured the maximum imaging depths of PAM. To test the penetration capability from the acoustic side, we placed a piece of 1.2-mm-thick chicken tissue between the ink sample and the ultrasonic transducer, whose working distance is 1.2 mm. The system impulse responses, both without and with the 1.2-mm chicken tissue, are shown in Fig. 4(a). With the 1.2-mm chicken tissue in place, the SNR decreases by 11 dB, and the pulse width broadens by 36%. Thus the axial resolution degrades approximately 36% because of the faster attenuation of the high-frequency ultrasound in the 1.2-mm chicken tissue. To test the penetration capability from the optical side, a human hair was inserted obliquely into chicken tissue. As shown in Fig. 4(b), the hair was imaged clearly with an SNR of ≥6 dB up to 0.44 mm deep in the tissue. However, deeper penetration is possible by using a lower NA optical objective.[19] Therefore, the PAM system can penetrate up to 0.44 mm into soft tissue from the optical side, limited by the SNR, and penetrate up to 1.2 mm from the acoustic side, limited by the working distance.

3.2 *High-Axial-Resolution Imaging*

Melanoma cells fixed by formalin were imaged by PAM *ex vivo*. The cells were seeded onto a slide at a density of 30 mm^{-2}. Two cross sections of a cell with 4-μm axial distance are shown in Fig. 5(a) and 5(b). The bright dots in the PAM images are melanosomes, the organelles containing melanin. The PAM images were validated by bright-field optical microscopy (0.75 NA, 20X; FV1000, Olympus), as shown in Fig. 5(c) and 5(d). The PAM image of the melanoma cell is rendered in 3-D as a video in Fig. 5(e).

Here the melanosomes can be approximated as point targets, so bright-field optical microscopy can provide 3-D images by depth scanning, though this approach would not work for planar targets.[22] Note that PAM generates a 3-D image without depth scanning. In Fig. 5(a)–5(d), the features of interest are indicated by the red dashed circles. The circled features are similar between the PAM and bright-field images, but they do not appear in the adjacent section. However, the difference between the PAM and bright-field images can still be observed, because in practice it is very difficult to take PAM and bright-field images exactly at the same depth and with the same sectioning angle.

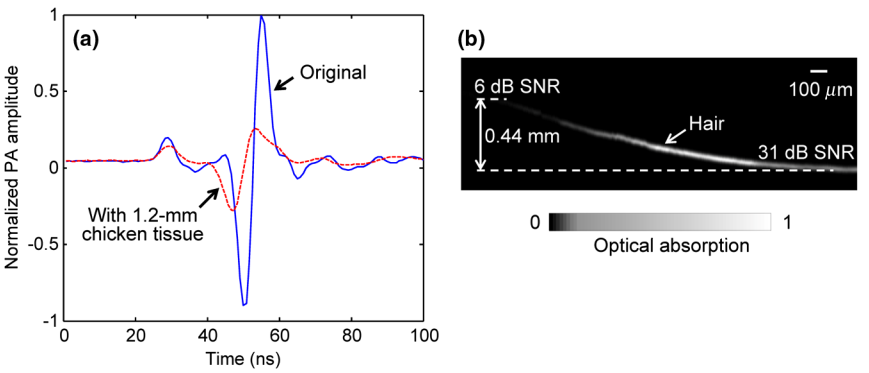

Fig. 4 Measuring the maximum imaging depths of PAM from both the acoustic and optical sides. (a) System impulse responses without (blue solid line) and with (red dashed line) 1.2-mm chicken tissue on the acoustic side. (b) A human hair inserted obliquely into chicken tissue from the optical side is imaged clearly up to 0.44 mm in depth.

The high-axial-resolution PAM was compared with a PAM system[23] with a 50 MHz ultrasonic transducer (90% bandwidth) by imaging mouse ears *in vivo*. The difference in axial resolution was expected to be >2 times. Both systems worked in transmission mode for a fair comparison. Depth-encoded maximum-amplitude projection (MAP) images of an ear from the two systems are shown in Fig. 6(a) and 6(b). Some blood vessels in the two images appear different, because the light was not focused at exactly the same depth in the ear in the two experiments. The side-view MAP images, as shown in Fig. 6(c) and 6(d), demonstrate the improvement in axial resolution. The high-axial-resolution PAM system with the 125 MHz ultrasonic transducer resolves the blood vessels much more clearly.

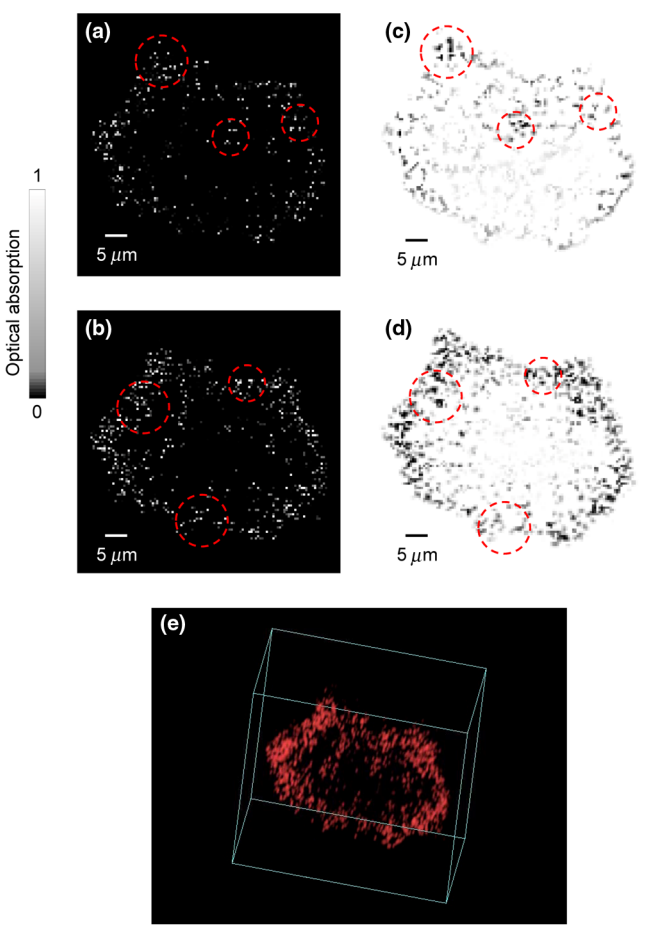

Fig. 5 Imaging of a melanoma cell. Two cross sections (with 4-μm axial distance) of the cell are imaged by (a,b) PAM and (c,d) bright-field optical microscopy, respectively. Red dashed circles indicate features for comparison. (e) 3-D PAM image (Video 1, MPEG, 3.9 MB) [URL: http://dx.doi.org/10.1117/1.JBO.17.11.116016.1]. The cuboid size is 60 μm by 60 μm by 30 μm.

4 Discussion and Conclusion

Detection sensitivity is a major concern when using a high-frequency ultrasonic transducer. In the *in vivo* mouse ear imaging experiment, the laser pulse energy was ~150 nJ. Assuming the optical focus was 80 μm beneath the skin surface, the surface laser fluence was 6.5 mJ $\cdot$ cm^{-2}, well below the American National Standards Institute (ANSI) safety limit of 20 mJ $\cdot$ cm^2, so the 125 MHz ultrasonic transducer is suitable for *in vivo* blood vessel imaging. It can be calculated from the results in Fig. 4(a) that the attenuation coefficient of ultrasound in the chicken tissue is 92 dB $\cdot$ cm^{-1}. For most soft tissues, the attenuation coefficient is nearly proportional to the acoustic frequency.[24] If the central frequency of the ultrasonic transducer is doubled, the acoustic penetration depth will decrease approximately 2 times. Therefore, challenges are expected if we want to further improve the axial resolution by simply using a higher-frequency ultrasonic transducer.

The deconvolution method used to improve the axial resolution has its limitations as well. Deconvolution should be applied to a linear and shift-invariant system. In PAM, as the laser intensity increases, the photoacoustic signal may become nonlinear with the laser intensity due to absorption saturation or nonlinear thermal expansion.[25] For oxyhemoglobin, the saturation intensity has been reported to be ~3×10^{12} W $\cdot$ m^{-2}.[25] With the nonlinear effects under such intensity, the deconvolution method may become invalid. In our *in vivo* experiments, the laser pulse energy is 150 nJ and the pulse width is 5 ns. If the optical focus is 80 μm beneath the skin surface and the extinction coefficient of the tissue is 100 cm^{-1}, light will attenuate ~55% at the optical focus according to Beer's law.[26] Then the intensity may exceed the saturation intensity within a ~7-μm depth range with the center at the optical focus. Moreover, the shift invariance holds accurately only within the focal zone of the ultrasonic transducer (~60 μm here) because the impulse response was measured at the acoustic focus. If a point target is far away from the acoustic focus in the depth direction, the received photoacoustic signal from the target will be quite different

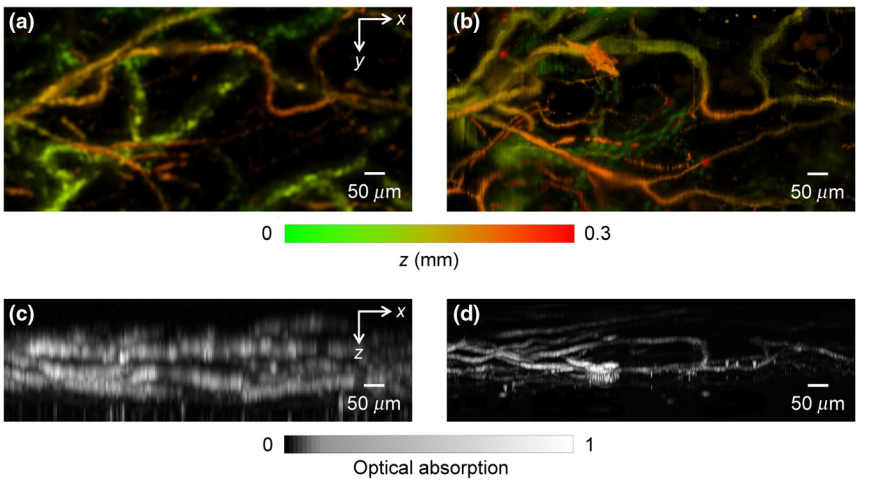

Fig. 6. Comparison of *in vivo* PAM images of a mouse ear acquired with 50 MHz and 125 MHz ultrasonic transducers. Depth-encoded PAM images acquired with the (a) 50 MHz and (b) 125 MHz ultrasonic transducers. Side-view PAM images acquired with the (c) 50 MHz and (d) 125 MHz ultrasonic transducers.

from the impulse response from the acoustic focus, causing errors in the deconvolution method. Taking Fig. 3(d) for example, the acoustic focus is approximately located at the bottom ink layer, which may be the major reason why the bottom layer appears thinner than the top layer in the deconvolved image. Here the top layer in Fig. 3(d) should still be located inside the acoustic focal zone, so the thickening of the top layer in the image may also indicate that either deconvolution starts to have error even within the acoustic focal zone or the acoustic focus is in fact slightly below the bottom layer. However, we can measure impulse responses at multiple axial positions and use time-variant-filtering inversion methods to ameliorate this problem.[27,28]

The acoustic lens for the ultrasonic transducer was made with a large NA of 0.8 in order to increase the solid angle of acoustic detection and thereby the SNR. Here, SNR is critical because the 125 MHz ultrasonic transducer has relatively low detection sensitivity, and high frequency ultrasound attenuates faster in biological tissue. The limitation associated with the high acoustic NA is the small depth of field (~60 μm), within which the acoustic amplitude degrades $<\sqrt{2}$ times compared with that at the focal point. Outside the acoustic focal zone, the SNR is weaker, and the axial resolution is lower. As shown by the results in Fig. 6(d), we could image blood vessels within a depth range of 150 μm, about 20 times the axial resolutions, with relatively good image quality.

Nonlinear effects in PAM can in fact be another mechanism to provide axial resolution other than the time-resolved ultrasonic detection. For example, two-photon-absorption induced PAM has been reported to achieve an optically determined axial resolution of 45 μm.[29] Theoretically, even submicron axial resolution is possible with a high-NA optical objective. However, for this technique, additional depth scanning is required as in two-photon microscopy,[30] which dramatically slows down image acquisition. In addition, due to the inefficiency of two-photon absorption at the ANSI-limited laser intensity, the two-photon-absorption signal may be weak.

In conclusion, an axial resolution of 7.6 μm, the finest thus far, has been achieved for PAM. The improved axial resolution benefits PAM in high-resolution 3-D imaging. We are extending the current system to reflection mode[14] for applications in more anatomical sites.

Appendix

Here we derived the axial resolution of PAM, which is limited by the acoustic bandwidth, when the impulse response $p(t)$ of the ultrasonic transducer is approximated as a Gaussian-modulated sinusoid:[31]

$$p(t) = A \exp\left(-\frac{(t-t_0)^2}{2\delta^2}\right)\cos(\omega_0 t + \phi), \qquad (1)$$

where t is time, A is the amplitude of impulse response, ω_0 is the transducer central frequency, and t_0, δ, and φ are constants. The axial resolution R_a is given by the corresponding distance of the FWHM of the temporal Gaussian envelope:

$$R_a = 2\sqrt{2\ln 2}\delta \cdot c, \qquad (2)$$

where c is the speed of sound.

The Fourier transformation of $p(t)$ is:

$$\hat{P}(\omega) = A\sqrt{\frac{\pi}{2}}\delta \exp\left[-i\omega\left(t_0 - \frac{\phi}{\omega_0}\right)\right] \cdot \left[\exp\left(-\frac{(\omega-\omega_0)^2\delta^2}{2}\right) + \exp\left(-\frac{(\omega+\omega_0)^2\delta^2}{2}\right)\right], \qquad (3)$$

where ω is the angular frequency. The acoustic -6 dB bandwidth B can be approximated by the FWHM of the Gaussian peak of $|\hat{P}(\omega)|$ at positive frequency:

$$B = \frac{2\sqrt{2\ln 2}}{\delta}(\text{rad/s}) \quad = \frac{\sqrt{2\ln 2}}{\pi\delta}(\text{Hz}). \qquad (4)$$

Combining Eqs. (2) and (4) leads to:

$$R_a = \frac{4 \ln 2}{\pi} \cdot \frac{c}{B} \approx 0.88 \frac{c}{B}. \quad (5)$$

Acknowledgments

We thank Prof. James Ballard for the close reading of the manuscript and Dr. Amy Winkler for helpful discussions. This work was sponsored in part by National Institutes of Health (NIH) grants R01 EB000712, R01 EB008085, R01 CA134539, U54 CA136398, R01 CA157277, and R01 CA159959. L.W. has a financial interest in Microphotoacoustics, Inc. and Endra, Inc., which, however, did not support this work. K.M. has a financial interest in Microphotoacoustics, Inc.

References

1. L. V. Wang and S. Hu, "Photoacoustic tomography: *in vivo* imaging from organelles to organs," *Science* **335**(6075), 1458–1462 (2012).
2. H. F. Zhang et al., "Functional photoacoustic microscopy for high-resolution and noninvasive *in vivo* imaging," *Nat. Biotech.* **24**(7), 848–851 (2006).
3. D.-K. Yao et al., "*In vivo* label-free photoacoustic microscopy of cell nuclei by excitation of DNA and RNA," *Opt. Lett.* **35**(24), 4139–4141 (2010).
4. C. Zhang et al., "Label-free photoacoustic microscopy of cytochrome *c* in cells," *Proc. SPIE* **8223**, 82231W (2012).
5. C. Zhang et al., "Label-free photoacoustic microscopy of myocardial sheet architecture," *J. Biomed. Opt.* **17**(6), 060506 (2012).
6. Y. Zhou et al., "Photoacoustic microscopy of bilirubin," *J. Biomed. Opt.* (submitted).
7. Z. Xu, Q. Zhu, and L. V. Wang, "*In vivo* photoacoustic tomography of mouse cerebral edema induced by cold injury," *J. Biomed. Opt.* **16**(6), 066020 (2011).
8. H.-W. Wang et al., "Label-free bond-selective imaging by listening to vibrationally excited molecules," *Phy. Rev. Lett.* **106**(23), 238106 (2011).
9. T. J. Allen et al., "Spectroscopic photoacoustic imaging of lipid-rich plaques in the human aorta in the 740 to 1400 nm wavelength range," *J. Biomed. Opt.* **17**(6), 061209 (2012).
10. J. Yao et al., "Label-free oxygen-metabolic photoacoustic microscopy *in vivo*," *J. Biomed. Opt.* **16**(7), 076003 (2011).
11. Y. Wang, K. Maslov, and L. V. Wang, "Spectrally encoded photoacoustic microscopy using a digital mirror device," *J. Biomed. Opt.* **17**(6), 066020 (2012).
12. J. Shah et al., "Photoacoustic imaging and temperature measurement for photothermal cancer therapy," *J. Biomed. Opt.* **13**(3), 034024 (2008).
13. C. Zhang, K. Maslov, and L. V. Wang, "Subwavelength-resolution label-free photoacoustic microscopy of optical absorption *in vivo*," *Opt. Lett.* **35**(19), 3195–3197 (2010).
14. C. Zhang et al., "Reflection-mode submicron-resolution *in vivo* photoacoustic microscopy," *J. Biomed. Opt.* **17**(2), 020501 (2012).
15. L. Wang et al., "Fast voice-coil scanning optical-resolution photoacoustic microscopy," *Opt. Lett.* **36**(2), 139–141 (2011).
16. Y. Wang et al., "Integrated photoacoustic and fluorescence confocal microscopy," *IEEE Trans. Biomed. Eng.* **57**(10), 2576–2578 (2010).
17. Z. Xie et al., "Pure optical photoacoustic microscopy," *Opt. Express* **19**(10), 9027–9034 (2011).
18. E. Z. Zhang et al., "Multimodal photoacoustic and optical coherence tomography scanner using an all optical detection scheme for 3-D morphological skin imaging," *Biomed. Opt. Express* **2**(8), 2202–2215 (2011).
19. S. Hu, K. Maslov, and L. V. Wang, "Second-generation optical-resolution photoacoustic microscopy with improved sensitivity and speed," *Opt. Lett.* **36**(7), 1134–1136 (2011).
20. J. A. Jensen et al., "Deconvolution of in-vivo ultrasound *B*-mode images," *Ultrason. Imag.* **15**(2), 122–133 (1993).
21. G. Ku et al., "Photoacoustic microscopy with 2-μm transverse resolution," *J. Biomed. Opt.* **15**(2), 021302 (2010).
22. L. V. Wang and H.-I. Wu, *Biomedical Optics: Principles and Imaging*, Wiley, Hoboken, New Jersey, pp. 164–169 (2007).
23. J. Yao et al., "Double-illumination photoacoustic microscopy," *Opt. Lett.* **37**(4), 659–662 (2012).
24. P. T. Wells, *Biomedical Ultrasonics*, pp. 120–123, Academic Press, New York (1977).
25. A. Danielli et al., "Picosecond absorption relaxation measured with nanosecond laser photoacoustics," *Appl. Phys. Lett.* **97**(16), 163701 (2010).
26. Y. Liu, C. Zhang, and L. V. Wang, "Effects of light scattering on optical-resolution photoacoustic microscopy," *J. Biomed. Opt.* (submitted).
27. S.-M. Phoong and P. P. Vaidyanathan, "Time-varying filters and filter banks: some basic principles," *IEEE Trans. Signal Process.* **44**(12), 2971–2987 (1996).
28. G. Wang, "The most general time-varying filter bank and time-varying lapped transforms," *IEEE Trans. Signal Process.* **54**(10), 3775–3789 (2006).
29. Y. Yamaoka, M. Nambu, and T. Takamatsu, "Fine depth resolution of two-photon absorption-induced photoacoustic microscopy using low-frequency bandpass filtering," *Opt. Express* **19**(14), 13365–13377 (2011).
30. F. Helmchen and W. Denk, "Deep tissue two-photon microscopy," *Nat. Methods* **2**(12), 932–940 (2005).
31. M. F. Insana and L. T. Cook, "Bioelasticity imaging: system design," *Proc. SPIE* **3659**, 224–235 (1999).